HHS Public Access

Author manuscript

Cancer Res. Author manuscript; available in PMC 2018 April 01.

Published in final edited form as:

Cancer Res. 2017 April 01; 77(7): 1719–1729. doi:10.1158/0008-5472.CAN-16-2159.

Systematic *in vivo* inactivation of chromatin regulating enzymes identifies Setd2 as a potent tumor suppressor in lung adenocarcinoma

David M. Walter[1,3], **Olivia S. Venancio**[1], **Elizabeth L. Buza**[6], **John W. Tobias**[4], **Charuhas Deshpande**[5], **A. Andrea Gudiel**[1], **Caroline Kim-Kiselak**[1], **Michelle Cicchini**[1], **Travis J. Yates**[1], and **David M. Feldser**[1,2,3,*]

[1]Department of Cancer Biology, University of Pennsylvania, Philadelphia, PA 19104

[2]Abramson Family Cancer Research Institute, University of Pennsylvania, Philadelphia, PA 19104

[3]Graduate Program in Cell and Molecular Biology, University of Pennsylvania, Philadelphia, PA 19104

[4]Department of Genetics and Penn Genomics Analysis Core, University of Pennsylvania, Philadelphia, PA 19104

[5]Department of Pathology & Laboratory Medicine, Perelman School of Medicine, University of Pennsylvania, Philadelphia, PA 19104

[6]Department of Pathobiology, School of Veterinary Medicine, University of Pennsylvania, Philadelphia, PA 19104

Abstract

Chromatin modifying genes are frequently mutated in human lung adenocarcinoma, but the functional impact of these mutations on disease initiation and progression is not well understood. Using a CRISPR-based approach, we systematically inactivated three of the most commonly mutated chromatin regulatory genes in two $Kras^{G12D}$-driven mouse models of lung adenocarcinoma to characterize the impact of their loss. Targeted inactivation of SWI/SNF nucleosome remodeling complex members *Smarca4* (*Brg1*) or *Arid1a* had complex effects on lung adenocarcinoma initiation and progression. Loss of either Brg1 or Arid1a were selected against in early stage tumors, but Brg1 loss continued to limit disease progression over time, whereas loss of Arid1a eventually promoted development of higher grade lesions. In contrast to these stage-specific effects, loss of the histone methyltransferase Setd2 had robust tumor promoting consequences. Despite disparate impacts of Setd2 and Arid1a loss on tumor development, each resulted in a gene expression profile with significant overlap. Setd2 inactivation and subsequent loss of H3K36me3 led to the swift expansion and accelerated progression of both early and late stage tumors. However, Setd2 loss *per se* was insufficient to overcome a p53-regulated barrier to malignant progression, nor establish the pro-metastatic cellular states that stochastically evolve during lung adenocarcinoma progression. Our study uncovers differential and context-dependent effects of SWI/SNF complex member loss, identifies Setd2 as a potent tumor suppressor in lung

*Correspondence: (215)898-9203, dfeldser@upenn.edu.

adenocarcinoma, and establishes model systems to facilitate further study of chromatin deregulation in lung cancer.

INTRODUCTION

Lung adenocarcinoma is the most common form of lung cancer in the U.S., and is characterized by poor survival and high mutation burdens [1, 2]. Although targeted therapies have been successfully developed for a subset of recurrently mutated genes such as EGFR, BRAF, and ALK, no such treatments exist for the vast majority of lung cancer patients [3]. A major obstacle to the development of additional targeted therapies is the unknown impact of commonly mutated genes on cancer progression and maintenance. Improved characterization, modeling, and validation of these cancer-associated genes will not only lead to a better understanding of the disease, but the ability to more effectively prioritize targets for future drug development.

The chromatin regulators *SMARCA4* (*BRG1*), *ARID1A*, and *SETD2* have been found to contain recurrent inactivating mutations in multiple tumor types including lung adenocarcinoma. These genes rank among the most commonly mutated genes in lung adenocarcinoma, occurring in ~25% of cases combined, and are typically mutated in a mutually exclusive manner (Supplementary Fig. S1A) [1]. Brg1 and Arid1a are components of the SWI/SNF chromatin remodeling complex which regulates gene expression through the ATP-dependent reorganization of nucleosome positioning [Reviewed in 4]. Brg1 is a core ATPase subunit of the complex, while Arid1a facilitates targeting of the complex through direct interaction with DNA and transcription factors [Reviewed in 4]. Loss of either Brg1 or Arid1a has been linked to multiple activities that promote cancer including pathological Myc signaling, defects in DNA repair, and impairment of cell cycle control [4–8]. While loss of Arid1a has yet to be studied in mouse models of lung adenocarcinoma, widespread loss of Brg1 in the lung limits tumor development in a model of carcinogen-induced lung adenocarcinoma. Conversely loss of Brg1 throughout the lung epithelium promoted the growth of established carcinogen-induced tumors [9]. Thus, loss of Brg1 is likely to have context-specific effects, but it remains unclear whether these effects of Brg1 loss are cancer cell autonomous or due to secondary effects of SWI/SNF disruption throughout lung tissue. While SWI/SNF complex components appear to play an important role in the suppression of lung adenocarcinoma, it is formally unknown whether their loss directly impacts the genesis of the disease [10]. Furthermore, it is unclear whether loss of individual complex members would have distinct effects on tumor progression that would indicate separable tumor suppressive programs controlled by distinct SWI/SNF complexes [11].

SETD2 is somatically mutated in a broad range of malignancies, including kidney, uterine, and bladder cancers, as well as lung adenocarcinoma [12]. *SETD2* encodes a histone methyltransferase that is unique in its ability to specifically catalyze histone H3 lysine 36 trimethylation (H3K36me3), and H3K36me3 is absent or dramatically reduced in cells that have lost normal Setd2 expression [13, 14]. H3K36me3 marks nucleosomes positioned along actively transcribed gene bodies, and its loss has been found to disrupt diverse

chromatin-related activities such as gene splicing, DNA repair, transcriptional elongation, DNA methylation, and maintenance of genome integrity [15, 16]. Despite strong correlative genetic evidence that Setd2 suppresses tumorigenesis, this has yet to be rigorously demonstrated *in vivo*.

Kras$^{LSL\text{-}G12D/+}$ and *Kras*$^{LSL\text{-}G12D/+}$;*p53*$^{flox/flox}$ mice form the basis of two well-characterized models of lung adenocarcinoma in which inhalation of Cre-expressing lentiviral vectors induces expression of oncogenic Kras^{G12D} alone, or in combination with p53 deletion in infected lung epithelial cells [17–19]. *Kras*$^{LSL\text{-}G12D/+}$ mice develop lung hyperplasias that efficiently expand to low-grade adenomas, and although progression to overt adenocarcinoma can occur in *Kras*$^{LSL\text{-}G12D/+}$ mice after long latency, the additional loss of p53 expression in the *Kras*$^{LSL\text{-}G12D/+}$;*p53*$^{flox/flox}$ model greatly facilitates the development of high-grade tumors and malignant progression [18]. As *KRAS* and *TP53* are the most frequently mutated genes in human lung adenocarcinoma, and often co-occur with mutations in *BRG1*, *ARID1A*, or *SETD2*, the *Kras*$^{LSL\text{-}G12D/+}$ and *Kras*$^{LSL\text{-}G12D/+}$;*p53*$^{flox/flox}$ models represent highly attractive and physiologically relevant systems to determine how loss of these chromatin regulators impacts tumor progression (Supplementary Fig. S1A–B).

Lentiviral-based CRISPR/Cas gene editing tools have emerged as a rapid and scalable method to discern biological effects of gene inactivation *in vivo* [20–23]. By incorporating Cas9 and sgRNA expression into Cre-expressing lentiviral vectors, it is now possible to inactivate genes in specific tissues within well-defined cancer models and investigate their effect on tumor formation and progression without expensive and time-consuming germline manipulations. Here we describe LentiCRISPRv2Cre, a Cas9, sgRNA, and Cre-expressing lentiviral vector based on an improved vector design to increase functional titers [24]. We used LentiCRISPRv2Cre to disrupt endogenous *Brg1*, *Arid1a*, or *Setd2* in both *Kras*$^{LSL\text{-}G12D/+}$ and *Kras*$^{LSL\text{-}G12D/+}$;*p53*$^{flox/flox}$ mouse models, and determined the impact of their loss during initiation and progression of lung adenocarcinoma.

MATERIALS AND METHODS

Vector Design and Production

The LentiCRISPRv2Cre vector was assembled using pSpCas9(BB)-2A–Puro V2.0 provided by Feng Zhang (Addgene plasmid #62988) as a backbone. Cre recombinase was PCR amplified using primers with overhangs that were complementary to pSpCas9(BB)-2A–Puro V2.0. The PCR product was then incorporated into pSpCas9(BB)-2A–Puro V2.0 using Gibson assembly (New England BioLabs E5510S) to create LentiCRISPRv2Cre. The BsmBI restriction site in Cre was mutated by site-directed mutagenesis. LentiCRISPRv2GFP was then assembled by PCR amplifying GFP with overhangs to LentiCRISPRv2Cre and incorporating this into the backbone by Gibson assembly. LentiCRISPRv2GFP (#82416) and LentiCRISPRv2Cre (#82415) are available from Addgene. sgRNAs were designed to target exons in the first third of the gene using the CRISPR Design Tool (http://crispr.mit.edu/about) to minimize off-target effects in the mouse genome. sgRNAs were cloned into LentiCRISPRv2Cre vector by Golden Gate assembly using BsmBI (New England BioLabs R0580S). The sgRNAs used for targeting Cas9 are:

Brg1, 5’-GGACGGCCTGTTGGTTGCGG-3’ or 5’-GGCATGTTCAGAGCCGCCGAGGG-3’, *Arid1a*, 5’-TGAGCGAGACTGCGCGACAC-3’ or 5’-GGTCCCTGTTGTTGCGAGTATGG-3’, and *Setd2*, 5’-AATGGGCTGAGGTACGCCGT-3’ or 5’-ATTCTGAACGGCGCTACCATAGG-3’. The sensor assay reporter was generated by synthesizing sgRNA targets in series and cloning them upstream of mCherry in the pCHK-mCherry vector using Gibson assembly.

Sensor Assay

HEK293 FT cells were purchased from Thermo Fisher, expanded and frozen after receipt, and used before passage 10. HEK293 FT cells were grown in DMEM (Gibco 10566-016) and plated into 6 well plates at 2×10^5 cells per well. Cells were transfected 24 hours later with 200 ng mCherry sensor reporter, 700 ng LentiCRISPRv2GFP backbone and 100 ng LentiCRISPRv2GFP containing sgRNA against the target or off-target control. The media was changed 16 hours post transfection. Mean fluorescence intensity of mCherry was measured by flow cytometry (Thermo Fisher Scientific Attune NxT Flow Cytometer) 72 hours post transfection, after gating on GFP positive cells. Mean fluorescence intensity was then normalized to the off-target control vector.

Lentivirus Production

HEK293 FT cells were transfected with LentiCRISPRv2Cre, Δ8.2 and VSV-G plasmids in a 4:3:1 ratio using polyethylenimine. 24 hours after transfection the media was replaced with fresh DMEM supplemented with 25 mM HEPES (Gibco 15630-080) and 3 mM caffeine (Sigma C0750). Lentivirus-containing supernatant was collected from the cells at 48 and 72 hours following transfection, filtered through 0.45 μm filters (Thermo Scientific 723–2545) and centrifuged at 107,000 g. The viral pellet was soaked in 100 μl PBS for 16 hours at 4°C, triturated, vortexed for 15 minutes at 4°C, and finally centrifuged at 16,000 g for 30 seconds to remove insoluble debris. Lentivirus was then aliquoted and frozen at −80°C for later use. Lentivirus was titered on Green-Go cells, an NIH3T3 derivative harboring an integrated Cre-dependent GFP reporter. These cells are validated for reporter activity by flow cytometry during viral titering. [21]. 2×10^5 cells were plated in 6 well plates, and 24 hours later lentivirus was added at 10, 1 and 0.1 ul per well. Cells were analyzed by flow cytometry for GFP expression 48 hours following infection, and viral titer was calculated accordingly.

Animal Work

All work was performed under compliance with Institutional Animal Care and Use Committee at the University of Pennsylvania (#804774). $Kras^{LSL\text{-}G12D}$ and $Kras^{LSL\text{-}G12D};p53^{flox/flox}$ mice are maintained on a mixed C567B6/129Sv4 background and were previously described [18]. Mice were given lentivirus at 6×10^4 pfu per mouse, or 1.2×10^4 pfu for survival studies, by intratracheal intubation at 6–10 weeks of age as previously described [19].

Immunohistochemistry and Immunofluorescence

Mouse tissues were fixed in 10% neutral buffered formalin (Fisher Scientific 23–245–685) for 16 hours and dehydrated in a series of ethanol washes up to 100%. Samples were

paraffin embedded and sectioned at 4μm thickness. Tissue microarrays were constructed using archival formalin fixed paraffin embedded tumor tissue blocks with institutional approval (IRB # 813643). For immunohistochemistry, slides were deparaffinized in xylene and rehydrated with a series of ethanol washes. Antigen retrieval was performed using citrate buffer (Electron Microscopy Sciences 62706-10) and slides were stained using antibodies against Arid1a (1:500, Sigma HPA005456), Brg1 (1:200, Santa Cruz sc-10768), H3K36me3 (1:1000, Abcam ab9050), p-H3 (1:500, Cell Signaling 9701), Cleaved Caspase-3 (1:200, Cell Signaling 9661), HMGA2 (1:300, BioCheck 59170AP), y-H2AX (1:200, Millipore 05–636), SPC (1:200, Millipore AB3786), CC10 (1:300, Santa Cruz sc-9772), and Nkx2-1 (1:250, Abcam Ab76013). Primary antibody was incubated on slides for 16 hours at 4°C, and biotinylated secondary antibody (Vector) was incubated at room temperature for 1 hour. ABC reagent and ImmPACT DAB were prepared as directed (Vector Laboratories PK-4001 and SK-4105). Slides were analyzed on a Leica DMI6000B inverted microscope. Tumors from mice were categorized as positive, mixed or negative for target protein expression according to the percent of positive staining cells by IHC. Positive tumors were marked as having greater than 75% positive cells, mixed tumors as having 25–75% positive cells, and negative tumors as having less than 25% positive cells.

Histological Analysis

Tumor number was counted on H&E stained slides. Tumor area was quantified using ImageJ software. Tumor grading was performed by a certified veterinary pathologist (E.L.B) using established tumor-grading schemes [18]. To quantify multinucleate giant cells, tissues were deparaffinized and stained with Fluoro-Gel II with DAPI (Electron Microscopy Sciences 17985-50). Individual nuclear sizes were measured using ImageJ.

Gene Expression Analysis

Tumor samples were micro-dissected away from normal lung tissue and RNA was extracted using Qiagen RNeasy Micro kit per manufacturers instructions. Sequencing libraries were prepared on the Illumina NeoPrep and subjected to 75 bp paired end sequencing on the Illumina NextSeq 500 platform. Fastq files for each sample were aligned against the mouse genome, build GRCm38.p4, using the STAR aligner (v2.5.2b) [25]. FeatureCounts (v1.5.0-p1) was used to quantify alignments against the mouse genomic annotations from Gencode (vM11) [26]. High purity of tumor cell derived RNA was estimated by detecting SNPs that were engineered during design of the $Kras^{LSL\text{-}G12D}$ allele in the Integrative Genomics Viewer [27, 28]. Differentially expressed genes were identified with DESeq2 (v1.14.0) [29].

Statistical Analysis

Statistical analyses were performed using GraphPad Prism software. Statistical analyses for sgRNA efficiency, tumor number, tumor area, proliferation and apoptotic rates, markers of DNA damage and frequency of multinucleate giant cells were performed using the student's T test. Significance in mouse tumor grading spectrum, occurrences of dedifferentiated cells or SPC^{-} $CC10^{+}$ cells, and human tissue sample analyses were determined with Chi-square analysis. Statistical analyses for mouse and human survival studies were performed using the Log-rank (Mantel-Cox) test.

RESULTS

LentiCRISPRv2Cre inactivates *Brg1*, *Arid1a*, and *Setd2* in *in vivo* models of Kras^{G12D}-driven lung adenocarcinoma

To inactivate genes of interest *in vivo*, we developed LentiCRISPRv2Cre, a variant of LentiCRISPRv2 that expresses Cre recombinase, Cas9, and a sgRNA targeting a gene of interest (Fig. 1A) [24]. In addition, we designed and validated high-efficiency sgRNAs targeting *Brg1*, *Arid1a*, and *Setd2* exonic sequences (Supplementary Fig. S2A–B). *Kras*$^{LSL\text{-}G12D/+}$ and *Kras*$^{LSL\text{-}G12D/+}$;*p53*$^{flox/flox}$ mice were then infected via inhalation of LentiCRISPRv2Cre expressing sgRNAs targeting either *Brg1*, *Arid1a*, *Setd2*, or GFP (Fig. 1A). Established tumors were assessed by immunohistochemistry for expression of Brg1, Arid1a, or H3K36me3 (an established marker of Setd2 activity)[13, 14]. LentiCRISPRv2Cre effectively eliminated Brg1 and Arid1a expression and H3K36me3 deposition in a subset of tumors, while other tumors retained expression or displayed a mixture of positively and negatively staining cells (Fig. 1B–D, Supplementary Fig. S3). Because CRISPR-mediated gene disruption is dependent on error-prone DNA repair after Cas9 nuclease activity, complete inactivation of target genes is not expected to occur in all tumors. To account for this tumor heterogeneity, we performed IHC on hundreds of individual tumors and developed an inclusive dataset to relate histological and molecular characteristics to the chromatin regulator status of each tumor. Ultimately this strategy allowed direct comparison of cancer phenotypes among positive, negative, and mixed staining tumors within mice.

Diverse effects on early stage lung adenomas after inactivation of *Brg1*, *Arid1a*, and *Setd2*

To assess the tumor suppressive potential of *Brg1*, *Arid1a*, and *Setd2* during early stage Kras^{G12D}-driven lung cancer, we examined tumors from *Kras*$^{LSL\text{-}G12D/+}$ mice 16 and 24 weeks after tumor initiation. Mice infected with LentiCRISPRv2Cre targeting *Arid1a* and *Setd2* had similar numbers of tumors compared to controls targeting GFP (Fig. 2A). Interestingly, the number of tumors identified in *Kras*$^{LSL\text{-}G12D/+}$ mice initiated with LentiCRISPRv2Cre targeting *Brg1* was notably decreased, though this difference did not achieve statistical significance (Fig. 2A). We also found that there was no significant difference in size between tumors that lost or retained expression of Brg1 or Arid1a (Fig. 2B). However, tumors that were negative or mixed for H3K36me3 were significantly larger and showed higher rates of proliferation, with no difference in rates of apoptosis, than tumors that maintained normal H3K36me3 levels (Fig. 2B, Supplementary Fig. S4A–B). The spectrum of tumor grades in *Kras*$^{LSL\text{-}G12D/+}$ mice were not affected by loss of Arid1a or Brg1 expression, but tumors with inactivated Setd2 displayed a shift towards more grade 2 adenomas (Fig. 2C). Interestingly, despite the clear increase in grade 2 adenomas after Setd2 inactivation, we never observed grade 3 tumors in *Kras*$^{LSL\text{-}G12D/+}$ mice at this time point (Fig. 2C). These results indicate that although loss of Setd2 promotes the growth of early stage lung adenomas by increasing proliferation rates, Setd2 loss alone is insufficient to overcome the p53-regulated barrier that suppresses the formation of grade 3 adenocarcinomas [30].

Loss of Arid1a or Setd2 significantly alters gene expression in Kras^{G12D}-driven tumors

To determine the impact that loss of chromatin regulating enzymes has on the global gene expression profile of nascent lung adenocarcinomas we performed RNA-Seq analysis on early stage lung adenomas from *Kras$^{LSL\text{-}G12D/+}$* mice. Isolation of Brg1 deficient Kras^{G12D}-driven tumors was not possible owing to the apparent selective disadvantage that its loss imposed on tumor development. We therefore focused on individual tumors that could be micro-dissected from the lungs of *Kras$^{LSL\text{-}G12D/+}$* mice that were initiated with LentiCRISPRv2Cre targeting either GFP, Arid1a, or Setd2. Tumors were fragmented and determined to be deficient for Setd2 or Arid1a by IHC prior to RNA isolation from the remaining tumor fragments (Supplementary Fig. S5A). We first analyzed the purity of the *Kras$^{G12D/+}$* tumor cells by determining the expressed allelic ratio of oncogenic versus wildtype *Kras* transcripts and found that more than half of the *Kras* transcripts were oncogenic, consistent with a high purity of tumor cells in all samples (Supplementary Fig. S5B). We then assessed global gene expression patterns between genotypes with principal component and pathway enrichment analyses (Fig. 3A and Supplementary Fig. S6) [31]. Although tumors with similar genotypes clustered together, Setd2 deficient tumors were dramatically separated from both Arid1a and GFP control tumors along the first principal component (PC#1, 19.5%, Fig. 3A). The expression profile of Arid1a deficient tumors was also distinct from GFP control tumors and was largely defined by the second principal component (PC#2, 12.5%, Fig. 3A). Whereas loss of Setd2 resulted in profound changes in the number of differentially expressed genes compared to GFP control tumors (>1500 genes), Arid1a deficient tumors had more modest changes (~500 genes) (Fig. 3B). However, despite the large difference in the total number of differentially expressed genes between Setd2 and Arid1a deficient tumors, the overlap of these genes was significantly larger than expected, suggesting that common pathways are deregulated by loss of these distinct chromatin regulators (Fig. 3B). Gene ontology pathways altered by both Setd2 and Arid1a loss were diverse and included pathways involved in cell movement, cytoskeleton, signaling, alternative splicing, and oxygen utilization (Supplementary Tables S1–3). These data demonstrate that while loss of Arid1a and Setd2 in Kras^{G12D}-driven lung cancer drives a dramatically different number of gene expression changes, many of these genes are altered in both conditions, and may potentially reveal pathways of tumor suppression that are shared amongst these mechanistically distinct chromatin regulating enzymes.

Opposing effects of chromatin regulator loss on the progression of high grade lung adenocarcinoma

To determine the impact of inactivating *Brg1*, *Arid1a*, and *Setd2* in combination with p53 loss in more advanced Kras^{G12D}-driven lung adenocarcinoma, we assessed tumors in *Kras$^{LSL\text{-}G12D/+}$;p53$^{flox/flox}$* mice 12 weeks after tumor initiation with LentiCRISPRv2Cre. Consistent with our observations in *Kras$^{LSL\text{-}G12D/+}$* mice expressing wildtype p53, we observed a comparable number of tumors in *Kras$^{LSL\text{-}G12D/+}$;p53$^{flox/flox}$* mice initiated with LentiCRISPRv2Cre targeting *Arid1a*, *Setd2*, and GFP (Fig. 4A). However, fewer tumors were present in mice infected with LentiCRISPRv2Cre targeting *Brg1* and these tumors demonstrated a significant increase in apoptotic rates, again suggesting that Brg1 is required for efficient tumor formation (Fig.4A, and Supplementary Figure S7A–B). While tumor size was unchanged in Arid1a or Brg1 mixed and negative tumors, tumors with mixed or no

H3K36me3 staining were significantly larger and had higher proliferation rates, with no change in the rate of apoptosis, than those that retained normal H3K36me3 levels (Fig. 4B and Supplementary Fig. S7A–B).

Lung tumors in *Kras*$^{LSL\text{-}G12D/+}$;*p53*$^{flox/flox}$ mice spontaneously acquire secondary alterations which can promote malignant progression (≥ grade 3) and development of a pro-metastatic state (grade 5) [30, 32]. Loss of Brg1 however did not promote the acquisition of advanced grade disease in *Kras*$^{LSL\text{-}G12D/+}$;*p53*$^{flox/flox}$ mice, but instead significantly increased the proportion of adenomatous alveolar hyperplasias (AAH) detected. The increase in AAH lesions is consistent with the persistence of the selective disadvantage of Brg1 loss in early lesions (Fig. 4C). In contrast to the subtle effects of targeting Arid1a in tumors expressing wildtype p53, loss of Arid1a significantly accelerated lung tumor progression in *Kras*$^{LSL\text{-}G12D/+}$;*p53*$^{flox/flox}$ mice. This suggests that the tumor suppressive roles of Arid1a are more apparent during later stages of tumor progression that occur in the absence of p53 (Fig. 4C). Inactivation of Setd2 also resulted in a dramatic shift in tumor grade, as the majority of H3K36me3 mixed and negative tumors were grade 3 or 4, in contrast to lower grade H3K36me3 positive tumors (Fig. 4C). However, we did not detect any gross metastases in these animals, and H3K36me3 negative tumors did not progress to a grade 5 poorly differentiated state within the 12 week experimental time course (Fig. 4C). This suggested that while Setd2 loss enables tumors to proliferate more rapidly and progress to higher grades, its inactivation does not directly trigger molecular programs responsible for development of grade 5 tumors previously shown to harbor metastatic potential [32, 33].

To determine whether loss of Brg1, Arid1a or Setd2 altered cellular fates after tumor initiation or during tumor progression as has been reported in other contexts [6, 34], we measured the expression of cellular lineage markers in extant tumors at early (8–12 week) and late (16 week) time points. Although multiple cell types in the mouse lung can initiate Kras^{G12D}-driven lung adenocarcinoma, all expanding tumors express surfactant protein C (SPC) and lack expression of club cell antigen 10 (CC10) [17, 35–38]. At early time points after tumor initiation we found that the overwhelming majority of tumors were SPC positive and CC10 negative, regardless of chromatin regulator status (Supplementary Fig. S8A). The development of poorly differentiated late stage metastatic disease (Grade 5), is marked by loss of the lung cell fate-determining transcription factor Nkx2-1 and derepression of Hmga2, an embryonic-restricted regulator of chromatin architecture [32, 33]. Sixteen weeks post tumor initiation we identified examples of these poorly differentiated, metastatic tumors, however their frequency was independent of Brg1, Arid1a, or Setd2 expression status (Supplementary Fig. S8B). This observation suggests that the general loss of chromatin regulators does not promote an increased rate of dedifferentiation, but that this is instead likely acquired through secondary genetic events.

Although tumors that had lost Setd2 activity were histopathologically representative of tumors from *Kras*$^{LSL\text{-}G12D/+}$ and *Kras*$^{LSL\text{-}G12D/+}$;*p53*$^{flox/flox}$ mice (Supplementary Fig. S9A) [18], they also displayed a distinctive, albeit subtle, morphological hallmark. At 12 and 16 weeks after tumor initiation in both *Kras*$^{LSL\text{-}G12D/+}$;*p53*$^{flox/flox}$ and *Kras*$^{LSL\text{-}G12D/+}$ mice respectively, H3K36me3 positive tumor cells are typically uniform, with minimal nuclear and cellular pleomorphism. In contrast, H3K36me3 negative tumor cells display severe

nuclear and cellular pleomorphism with increased nuclear to cytoplasmic ratio (Supplementary Fig. S9B). Additionally, Setd2 deficient tumors had more frequent multinucleate giant cells and aberrant mitoses than tumors from mice given LentiCRISPRv2Cre targeting GFP (Supplementary Fig. S10A–C). These mitotic defects are consistent with a recent report demonstrating the unanticipated activity of Setd2 in the methylation of α-tubulin to regulate proper cytokinesis [16].

Loss of Arid1a and Setd2 are selected over time

To rigorously assess the tumor suppressive potential of *Brg1*, *Arid1a*, and *Setd2* in lung adenocarcinoma, we analyzed the selective advantage conferred by loss of each of these chromatin modifiers on tumor progression. We examined lung tumors from $Kras^{LSL\text{-}G12D/+};p53^{flox/flox}$ mice infected with LentiCRISPRv2Cre targeting *Brg1*, *Arid1a*, or *Setd2* at 8, 12, and 16 weeks post tumor initiation. We then quantified the percent of tumors with positive, mixed or negative target protein expression at each time point by IHC (Fig. 5A–C). Consistent with a requirement for SWI/SNF complex function during early tumor development in $Kras^{LSL\text{-}G12D/+};p53^{flox/flox}$ mice, no Brg1 or Arid1a negative tumors were detected at 8 weeks after initiation (Fig. 5A–B). Although the incidence of lesions that had mixed or negative staining for Brg1 and Arid1a increased over time, lesions lacking Brg1 expression which later emerged were always low grade tumors or AAH (Fig. 5A). In contrast, while the population of tumors lacking Arid1a 16 weeks after tumor initiation still represented a minority of all tumors, those that were present were often high grade tumors (Fig. 5B). These observations suggest that SWI/SNF complex functions controlled by Brg1 are continuously required after tumor initiation, whereas loss of SWI/SNF complex functions controlled by Arid1a is selected for over time and plays an important role in driving tumor progression.

In comparison, partial or complete Setd2 deficiency was observed in >50% of tumors eight weeks after tumor initiation. The proportion of Setd2 deficient tumors also steadily increased from 56% to 79% to 94% at 8, 12, and 16 week time points respectively, indicating that Setd2 deficient tumors outcompete those that maintain normal H3K36me3 levels (Fig. 5C). These data demonstrate that the activity of Setd2 is strongly tumor suppressive and is continually selected during lung adenocarcinoma progression.

Loss of Setd2 activity decreases overall survival and is frequently associated with human *KRAS* mutant lung adenocarcinomas

The strong selective advantage of Setd2 loss allowed the accurate determination of the overall impact that Setd2 loss has on survival. $Kras^{LSL\text{-}G12D/+};p53^{flox/flox}$ mice infected with LentiCRISPRv2Cre targeting Setd2 became moribund and required euthanasia significantly sooner than GFP control cohorts (Fig. 6A). These data reflect patient outcomes for human LUAD, for whom low Setd2 expression is associated with dramatically reduced overall survival (Fig. 6B)[39]. To further demonstrate the relationship between *SETD2* loss and lung adenocarcinoma amongst human patient samples, we stained 60 human tumors (~6 cores per tumor sample) with known *KRAS* or *EGFR* mutations for H3K36me3 deposition (Fig. 6C). We found that 20 out of 60 (33%) lung adenocarcinomas exhibited low to negative staining for H3K36me3. Interestingly, we found that *KRAS* mutant tumors were

significantly more likely than *EGFR* mutant tumors to have reduced or absent staining for H3K36me3 (p=0.02, Fig. 6D). These observations indicate that H3K36me3 loss is a prevalent feature of human lung adenocarcinoma that co-occurs with *KRAS* mutation at high frequency.

DISCUSSION

Cancer genome sequencing studies of diverse malignancies have uncovered a surprising enrichment of mutations in genes that regulate chromatin structure and function. Yet determining the functional role that each of these mutations has on cancer initiation and progression has remained daunting. CRISPR/Cas gene editing technologies now permit the rapid and systematic assessment of multiple mutations within relevant cancer model systems [21, 40]. In lung adenocarcinoma, *BRG1*, *ARID1A*, and *SETD2* are amongst the most commonly mutated genes. The specific mutations are spread across the gene body and frequently result in nonsense and frameshift alterations consistent with gene inactivation [1, 12]. Based on this human sequencing data, mutations of these chromatin regulators were predicted to facilitate lung adenocarcinoma development. However, we observed that inactivation of these genes *in vivo* had variable effects on tumor initiation and progression.

The SWI/SNF complex is a multi-protein chromatin regulation complex that modulates gene expression by regulating DNA accessibility, and is a frequent target of somatic mutation in human cancers [4]. Despite the high frequency of *BRG1* and *ARID1A* mutations in human lung adenocarcinoma, we were unable to detect tumors that had lost Brg1 and few that had lost Arid1a expression during the earliest stages of tumor initiation, demonstrating that SWI/SNF chromatin remodeling activity is required at early disease stages. While loss of Brg1 continued to limit tumor progression at later time points, we observed a significant increase in the incidence of more advanced lesions that had lost Arid1a expression in $Kras^{LSL\text{-}G12D/+};p53^{flox/flox}$ tumors. That *ARID1A* mutations are present in these early lesions in the mouse, but do not act as a significant driver of tumor progression in those cells, is consistent with the recent identification of *ARID1A* mutations in incidental pre-neoplastic lesions discovered in lung resection patients [41]. This suggests that once tumors attain a cellular state associated with more advanced disease, loss of Arid1a promotes disease progression. Thus, the loss of SWI/SNF complex function has opposing effects on the progression of lung adenocarcinoma at distinct stages of the disease and these tumor suppressive effects are differentially regulated by distinct members of the complex. These context-specific roles are interesting in light of work in $Kras^{G12D}$-driven pancreatic cancer models, where loss of Brg1 expression opposes the development of one disease subtype but promotes the development of another depending on the initiating cell of origin and the stage of tumor progression [42]. However in the lung adenocarcinoma model used here, we were unable to detect any changes in the initiating cell type, anatomic location of developing tumors, or in the differentiation state of extant tumors regardless of their underlying genetic mutation status. Because of the strong selective disadvantage of SWI/SNF deregulation during early stages of tumor initiation in our model, systems which limit inactivation of SWI/SNF complex members to tumors after they are established are needed to better understand the individual role each complex member plays in particular stages of tumor progression.

In contrast to the modest effects of SWI/SNF complex mutations, CRISPR-mediated disruption of *Setd2* profoundly affected $Kras^{G12D}$-driven tumors in the lung. Tumors lacking Setd2 had significantly increased cell proliferation rates, resulting in much larger and more rapidly progressing tumors compared to controls. Furthermore, these tumor promoting effects of Setd2 loss were evident in both p53 deficient tumors and tumors from $p53^{+/+}$ mice. However, despite the rapid expansion and progression of tumors upon Setd2 inactivation, these tumors were still limited by well-defined progression checkpoints characteristic of the $Kras^{LSL\text{-}G12D/+}$ and $Kras^{LSL\text{-}G12D/+};p53^{flox/flox}$ tumor models. The transition to malignancy (grade 3) is opposed by the p53 pathway in $Kras^{G12D/+}$ lung tumors, and within the 16 week time course of our experiments, Setd2 loss was not sufficient to overcome this barrier to malignant lung tumor progression [18, 30]. In $Kras^{LSL\text{-}G12D/+};p53^{flox/flox}$ tumors, Setd2 loss promoted rapid tumor progression and expansion up to grade 4, but did not promote progression to grade 5 status in the 12 weeks after initiation. Additionally, at 16 weeks post tumor initiation in $Kras^{LSL\text{-}G12D/+};p53^{flox/flox}$ mice, Hmga2-expressing grade 5 tumors that had lost H3K36me3 were readily detected; however these did not occur at increased frequency compared to H3K36me3 positive tumors. Thus, Setd2 loss promotes the rapid growth and progression of tumors in a manner that is independent of p53, but is still subject to the tumor suppressive constraints of p53- and Nkx2-1/Hmga2-regulated progression checkpoints [30, 32].

The precise mechanism by which Setd2 loss promotes tumor progression remains unclear, however our analysis of differential gene expression in tumors that have lost Setd2 activity sheds some light on possible mechanisms. Defects in chromosome segregation, DNA repair, and reduced nucleotide pools have been observed in cultured cells that have lost Setd2 expression, which sensitizes these lines to inhibition of DNA damage checkpoints [16, 43, 44]. We found no difference in markers of DNA double strand breaks (γ-H2AX) or apoptosis (cleaved caspase 3). However, GO terms that emerged from our RNA-Seq analyses included microtubule, cytoskeleton, and motor protein, which could result in defective cytokinesis. Additionally, tumors lacking Setd2 activity had prevalent aberrant mitotic figures and multinucleate giant cells, indicating that DNA replication/repair or mitotic defects are likely present in these tumors. Yet these defects likely limit cell fitness, and thus appear to be at odds with the immediate and widespread proliferation that occurs with Setd2 loss in tumors. In light of the distinct overlap of differentially expressed genes regulating alternative splicing in both Arid1a and Setd2 deficient tumors, and the common occurrence of somatic alterations in spliceosomal components across multiple cancer types [45], it is intriguing to speculate that defective alternative splicing could be a common driving force of tumor progression after loss of proper chromatin regulation. Further study of the signaling pathways and gene expression programs altered in these $Kras^{G12D}$-driven tumors will be necessary to understand the mechanisms linking chromatin regulator loss and tumor progression. Finally, to our knowledge our study is the first evidence that Setd2 loss functionally contributes to the *in vivo* growth and progression of lung adenocarcinoma, and establishes Setd2 as a bona fide tumor suppressor in this disease.

Supplementary Material

Refer to Web version on PubMed Central for supplementary material.

Acknowledgments

We would like to extend a special thanks to J. Ludwig and the ULAR animal husbandry staff, and to J. Wang, Q-C. Yu, and other members of the histology core staff for their technical expertise. Thanks to I. Asangani and P. Gollavilli for help with sequencing library preparation and NextGen sequencing, N. Joshi for Green-Go cells, and W. Wang and E. Witze for the pCHK-mCherry vector, and K. Stokes for technical assistance. Finally, we thank C. Harrington for critical reading of this manuscript. This work was supported by an American Association for Cancer Research-Bayer HealthCare Basic Cancer Research Fellowship (M.C.), grants from the National Institute of Health; R00-CA158581 and R01-CA193602 (to D.M.F), T32ES019851 (to M.C.) and P30-CA016520 (Penn Abramson Cancer Center), and in part by the University of Pennsylvania's Undergraduate Research Mentorship program (O.V). This work is dedicated to memory of Dr. Qian-Chun Yu and his caring leadership of the histopathology core of the Department of Cancer Biology and Abramson Family Cancer Research Institute.

Financial Support: D.M. Feldser is supported by NIH R00-CA158581, R01-CA193602, R21-CA205340, and from the American Lung Association LCD400095. M. Cicchini was supported by the Association for Cancer Research-Bayer HealthCare Basic Cancer Research Fellowship, and Center of Excellence in Environmental Toxicology T32 training grant T32ES019851, O.S. Venancio, was supported by the University of Pennsylvania's Undergraduate Research Mentorship program, T.J. Yates is supported by the American Cancer Society, North Texas Pay If Group Postdoctoral Fellowship, PF-16-22401TBE, and all authors are supported by the Penn Abramson Cancer Center core grant P30-CA016520. The authors disclose no potential conflicts of interest.

References

1. Comprehensive molecular profiling of lung adenocarcinoma. Nature. 2014; 511(7511):543–550. [PubMed: 25079552]
2. Cancer Facts & Figures 2015. Atlanta: American Cancer Society; 2015.
3. Reck M, et al. Management of non-small-cell lung cancer: recent developments. Lancet. 2013; 382(9893):709–719. [PubMed: 23972814]
4. Wilson BG, Roberts CW. SWI/SNF nucleosome remodellers and cancer. Nat Rev Cancer. 2011; 11(7):481–492. [PubMed: 21654818]
5. Strobeck MW, et al. BRG-1 is required for RB-mediated cell cycle arrest. Proc Natl Acad Sci U S A. 2000; 97(14):7748–7753. [PubMed: 10884406]
6. Romero OA, et al. The tumour suppressor and chromatin-remodelling factor BRG1 antagonizes Myc activity and promotes cell differentiation in human cancer. EMBO Mol Med. 2012; 4(7):603–616. [PubMed: 22407764]
7. Zhang L, et al. The chromatin remodeling protein BRG1 modulates BRCA1 response to UV irradiation by regulating ATR/ATM activation. Front Oncol. 2013; 3:7. [PubMed: 23346553]
8. Watanabe R, et al. SWI/SNF factors required for cellular resistance to DNA damage include ARID1A and ARID1B and show interdependent protein stability. Cancer Res. 2014; 74(9):2465–2475. [PubMed: 24788099]
9. Glaros S, et al. Targeted knockout of BRG1 potentiates lung cancer development. Cancer Res. 2008; 68(10):3689–3696. [PubMed: 18483251]
10. Arron JR, et al. NFAT dysregulation by increased dosage of DSCR1 and DYRK1A on chromosome 21. Nature. 2006; 441(7093):595–600. [PubMed: 16554754]
11. Kadoch C, Crabtree GR. Mammalian SWI/SNF chromatin remodeling complexes and cancer: Mechanistic insights gained from human genomics. Sci Adv. 2015; 1(5):e1500447. [PubMed: 26601204]
12. Cerami E, et al. The cBio cancer genomics portal: an open platform for exploring multidimensional cancer genomics data. Cancer Discov. 2012; 2(5):401–404. [PubMed: 22588877]
13. Sun XJ, et al. Identification and characterization of a novel human histone H3 lysine 36-specific methyltransferase. J Biol Chem. 2005; 280(42):35261–35271. [PubMed: 16118227]
14. Li J, et al. SETD2: an epigenetic modifier with tumor suppressor functionality. Oncotarget. 2016
15. Edmunds JW, Mahadevan LC, Clayton AL. Dynamic histone H3 methylation during gene induction: HYPB/Setd2 mediates all H3K36 trimethylation. EMBO J. 2008; 27(2):406–420. [PubMed: 18157086]

16. Park IY, et al. Dual Chromatin and Cytoskeletal Remodeling by SETD2. Cell. 2016; 166(4):950–962. [PubMed: 27518565]
17. Jackson EL, et al. Analysis of lung tumor initiation and progression using conditional expression of oncogenic K-ras. Genes Dev. 2001; 15(24):3243–3248. [PubMed: 11751630]
18. Jackson EL, et al. The differential effects of mutant p53 alleles on advanced murine lung cancer. Cancer Res. 2005; 65(22):10280–10288. [PubMed: 16288016]
19. DuPage M, Dooley AL, Jacks T. Conditional mouse lung cancer models using adenoviral or lentiviral delivery of Cre recombinase. Nat Protoc. 2009; 4(7):1064–1072. [PubMed: 19561589]
20. Hsu PD, Lander ES, Zhang F. Development and Applications of CRISPR-Cas9 for Genome Engineering. Cell. 2014; 157(6):1262–1278. [PubMed: 24906146]
21. Sanchez-Rivera FJ, et al. Rapid modelling of cooperating genetic events in cancer through somatic genome editing. Nature. 2014
22. Xue W, et al. CRISPR-mediated direct mutation of cancer genes in the mouse liver. Nature. 2014; 514(7522):380–384. [PubMed: 25119044]
23. Chiou SH, et al. Pancreatic cancer modeling using retrograde viral vector delivery and in vivo CRISPR/Cas9-mediated somatic genome editing. Genes Dev. 2015; 29(14):1576–1585. [PubMed: 26178787]
24. Sanjana NE, Shalem O, Zhang F. Improved vectors and genome-wide libraries for CRISPR screening. Nat Methods. 2014; 11(8):783–784. [PubMed: 25075903]
25. Dobin A, et al. STAR: ultrafast universal RNA-seq aligner. Bioinformatics. 2013; 29(1):15–21. [PubMed: 23104886]
26. Liao Y, Smyth GK, Shi W. featureCounts: an efficient general purpose program for assigning sequence reads to genomic features. Bioinformatics. 2014; 30(7):923–930. [PubMed: 24227677]
27. Tuveson DA, et al. Endogenous oncogenic K-ras(G12D) stimulates proliferation and widespread neoplastic and developmental defects. Cancer Cell. 2004; 5(4):375–387. [PubMed: 15093544]
28. Thorvaldsdottir H, Robinson JT, Mesirov JP. Integrative Genomics Viewer (IGV): high-performance genomics data visualization and exploration. Brief Bioinform. 2013; 14(2):178–192. [PubMed: 22517427]
29. Love MI, Huber W, Anders S. Moderated estimation of fold change and dispersion for RNA-seq data with DESeq2. Genome Biol. 2014; 15(12):550. [PubMed: 25516281]
30. Feldser DM, et al. Stage-specific sensitivity to p53 restoration during lung cancer progression. Nature. 2010; 468(7323):572–575. [PubMed: 21107428]
31. Jolliffe IT, Cadima J. Principal component analysis: a review and recent developments. Philos Trans A Math Phys Eng Sci. 2016; 374(2065):20150202. [PubMed: 26953178]
32. Winslow MM, et al. Suppression of lung adenocarcinoma progression by Nkx2-1. Nature. 2011; 473(7345):101–104. [PubMed: 21471965]
33. Li CM, et al. Foxa2 and Cdx2 cooperate with Nkx2-1 to inhibit lung adenocarcinoma metastasis. Genes Dev. 2015; 29(17):1850–1862. [PubMed: 26341558]
34. Oike T, et al. A synthetic lethality-based strategy to treat cancers harboring a genetic deficiency in the chromatin remodeling factor BRG1. Cancer Res. 2013; 73(17):5508–5518. [PubMed: 23872584]
35. Kim CF, et al. Identification of bronchioalveolar stem cells in normal lung and lung cancer. Cell. 2005; 121(6):823–835. [PubMed: 15960971]
36. Xu X, et al. Evidence for type II cells as cells of origin of K-Ras-induced distal lung adenocarcinoma. Proceedings of the National Academy of Sciences of the United States of America. 2012; 109(13):4910–4915. [PubMed: 22411819]
37. Rowbotham SP, Kim CF. Diverse cells at the origin of lung adenocarcinoma. Proc Natl Acad Sci U S A. 2014; 111(13):4745–4746. [PubMed: 24707043]
38. Sutherland KD, et al. Multiple cells-of-origin of mutant K-Ras-induced mouse lung adenocarcinoma. Proceedings of the National Academy of Sciences of the United States of America. 2014; 111(13):4952–4957. [PubMed: 24586047]

39. Gyorffy B, et al. Online survival analysis software to assess the prognostic value of biomarkers using transcriptomic data in non-small-cell lung cancer. PloS one. 2013; 8(12):e82241. [PubMed: 24367507]

40. Caswell DR, et al. Obligate progression precedes lung adenocarcinoma dissemination. Cancer discovery. 2014; 4(7):781–789. [PubMed: 24740995]

41. Izumchenko E, et al. Targeted sequencing reveals clonal genetic changes in the progression of early lung neoplasms and paired circulating DNA. Nat Commun. 2015; 6:8258. [PubMed: 26374070]

42. Roy N, et al. Brg1 promotes both tumor-suppressive and oncogenic activities at distinct stages of pancreatic cancer formation. Genes Dev. 2015; 29(6):658–671. [PubMed: 25792600]

43. Pfister SX, et al. SETD2-dependent histone H3K36 trimethylation is required for homologous recombination repair and genome stability. Cell Rep. 2014; 7(6):2006–2018. [PubMed: 24931610]

44. Pfister SX, et al. Inhibiting WEE1 Selectively Kills Histone H3K36me3-Deficient Cancers by dNTP Starvation. Cancer Cell. 2015; 28(5):557–568. [PubMed: 26602815]

45. Sveen A, et al. Aberrant RNA splicing in cancer; expression changes and driver mutations of splicing factor genes. Oncogene. 2016; 35(19):2413–2427. [PubMed: 26300000]

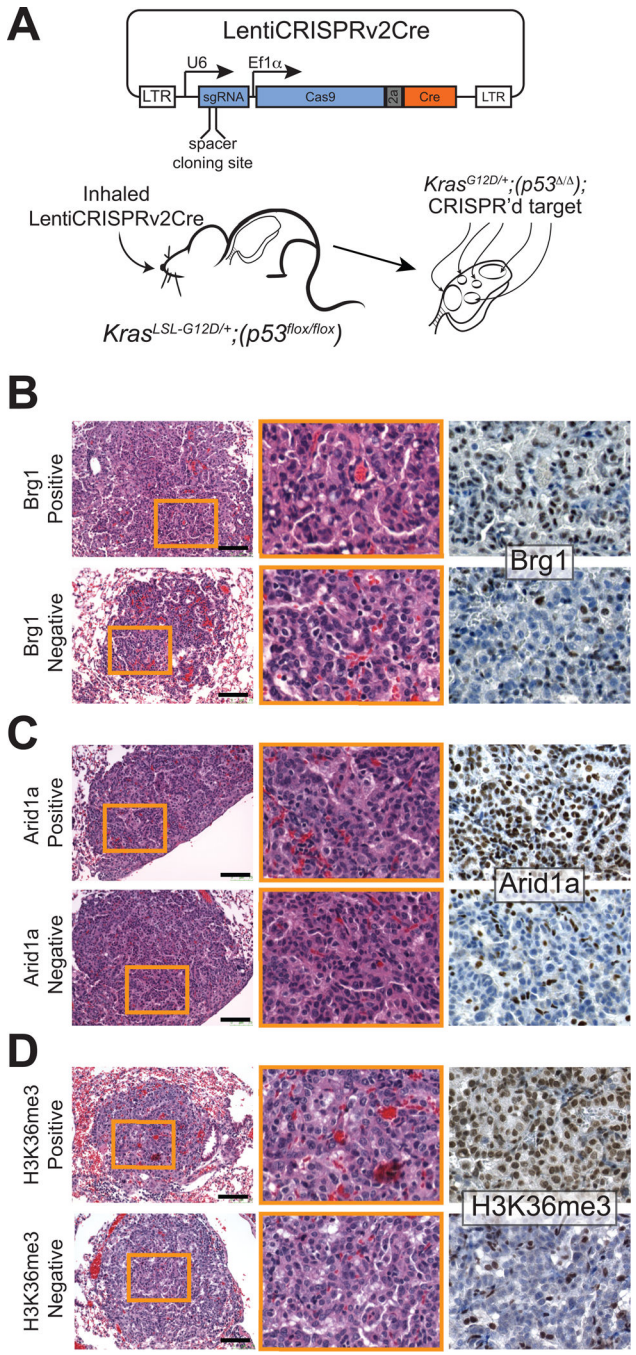

Figure 1.

LentiCRISPRv2Cre induces target gene inactivation *in vivo*. a) Diagram of the LentiCRISPRv2Cre vector and depiction of lentiviral lung tumor induction concurrent with chromatin regulator loss. b-d) H&E and immunohistochemistry images for b) Brg1, c) Arid1a, and d) H3K36me3 12 weeks following LentiCRISPRv2Cre infection in $Kras^{LSL\text{-}G12D/+};p53^{flox/flox}$ mice. Left panels: H&E low magnification image of tumor, middle panels: H&E high magnification image of indicated region, right panels: chromatin regulator or histone mark IHC for indicated region. Scale bars= 100 μm.

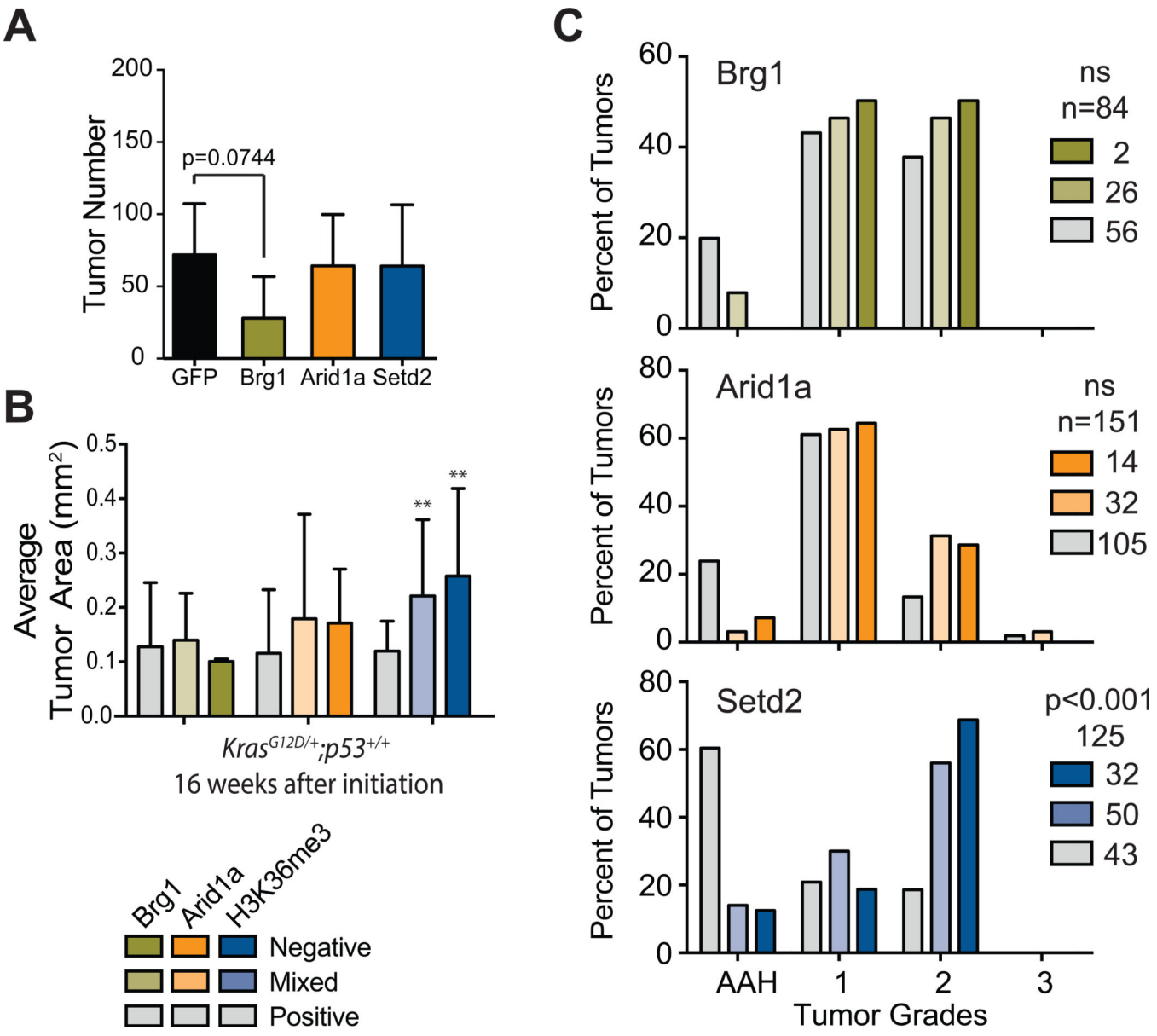

Figure 2.

Inactivation of Brg1, Arid1a, and Setd2 in *Kras*$^{LSL\text{-}G12D/+}$ mice. a) Tumor number quantification in lungs 16 weeks following infection with LentiCRISPRv2Cre targeting GFP (n=6), *Brg1* (n=4), *Arid1a* (n=5), or *Setd2* (n=7). b) Average tumor area of Brg1, Arid1a, and H3K36me3 positive, mixed and negative tumors in *Kras*$^{LSL\text{-}G12D/+}$ mice 16 weeks following infection with LentiCRISPRv2Cre, **p<0.01. c) Tumor grading for Brg1 (upper), Arid1a (middle), and H3K36me3 (lower) positive, mixed and negative tumors, in *Kras*$^{LSL\text{-}G12D/+}$ mice 16 weeks following infection with LentiCRISPRv2Cre. AAH= atypical adenomatous hyperplasia.

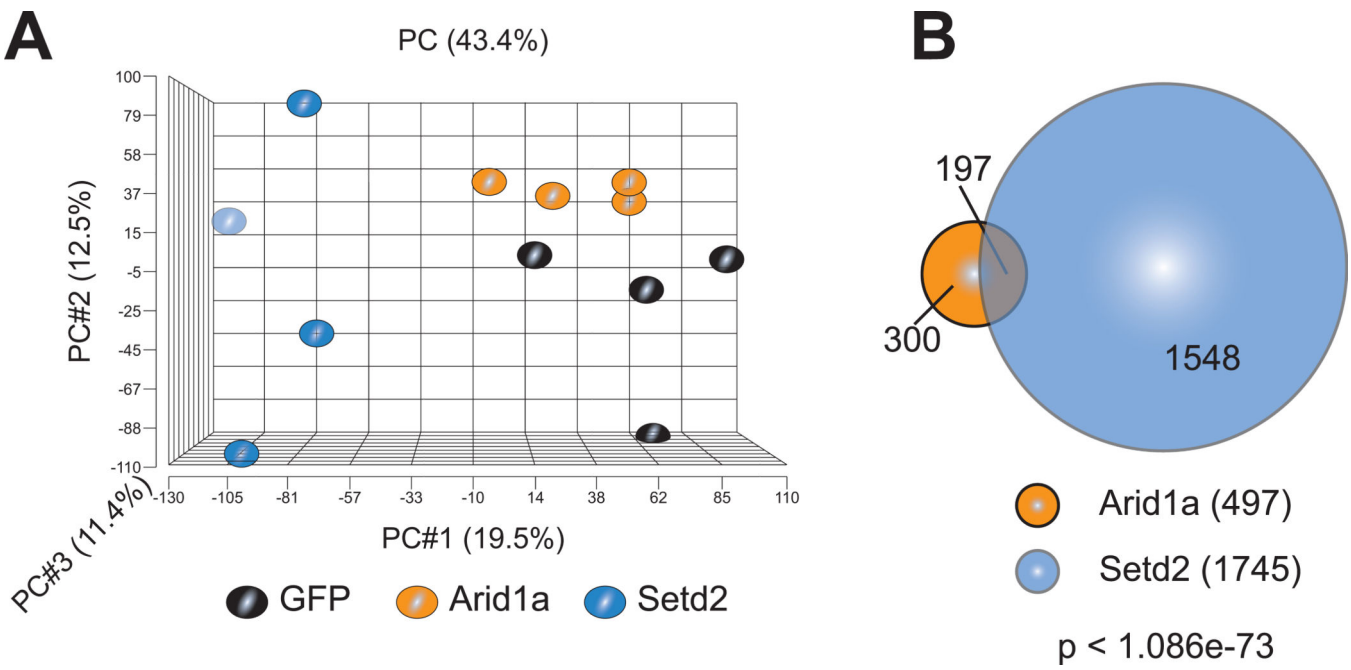

Figure 3.

Arid1a and Setd2 deficient tumors have distinct gene expression profiles and share a significant overlap in differentially expressed genes in *Kras*$^{LSL\text{-}G12D/+}$ mice. a) Principal component analysis of tumors initiated with LentiCRISPRv2Cre targeting GFP (n=4), *Arid1a* (n=4) or *Setd2* (n=4). b) Number of differentially regulated genes in Arid1a deficient tumors alone, Setd2 deficient tumors alone or both groups. Cutoff for differentially expressed genes set as FC>±0.8 and p<0.05.

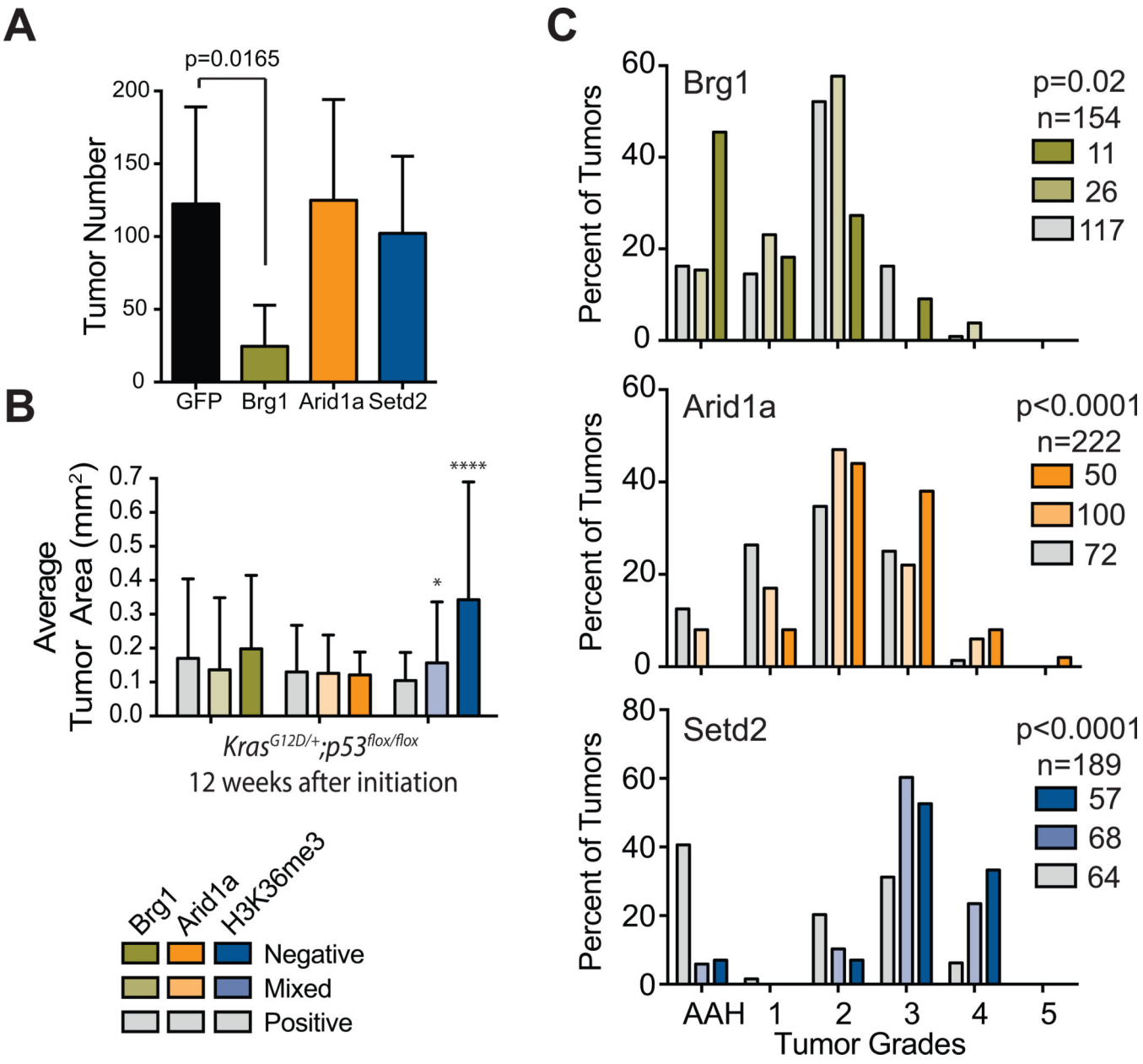

Figure 4.

Inactivation of Brg1, Arid1a, and Setd2 in *Kras*$^{LSL\text{-}G12D/+}$; *p53*$^{flox/flox}$ mice. a) Tumor number quantification in lungs 12 weeks following infection with LentiCRISPRv2Cre targeting GFP (n=5), *Brg1* (n=5), *Arid1a* (n=6) or *Setd2* (n=5). b) Average tumor area of Brg1, Arid1a and H3K36me3 positive, mixed and negative tumors, in *Kras*$^{LSL\text{-}G12D/+}$;*p53*$^{flox/flox}$ mice 12 weeks following infection with LentiCRISPRv2Cre, *p<0.05, ****p<0.0001. c) Tumor grading for Brg1 (upper), Arid1a (middle) and H3K36me3 (lower) positive, mixed and negative tumors, in *Kras*$^{LSL\text{-}G12D/+}$;*p53*$^{flox/flox}$ mice 12 weeks following infection with LentiCRISPRv2Cre. AAH= atypical adenomatous hyperplasia.

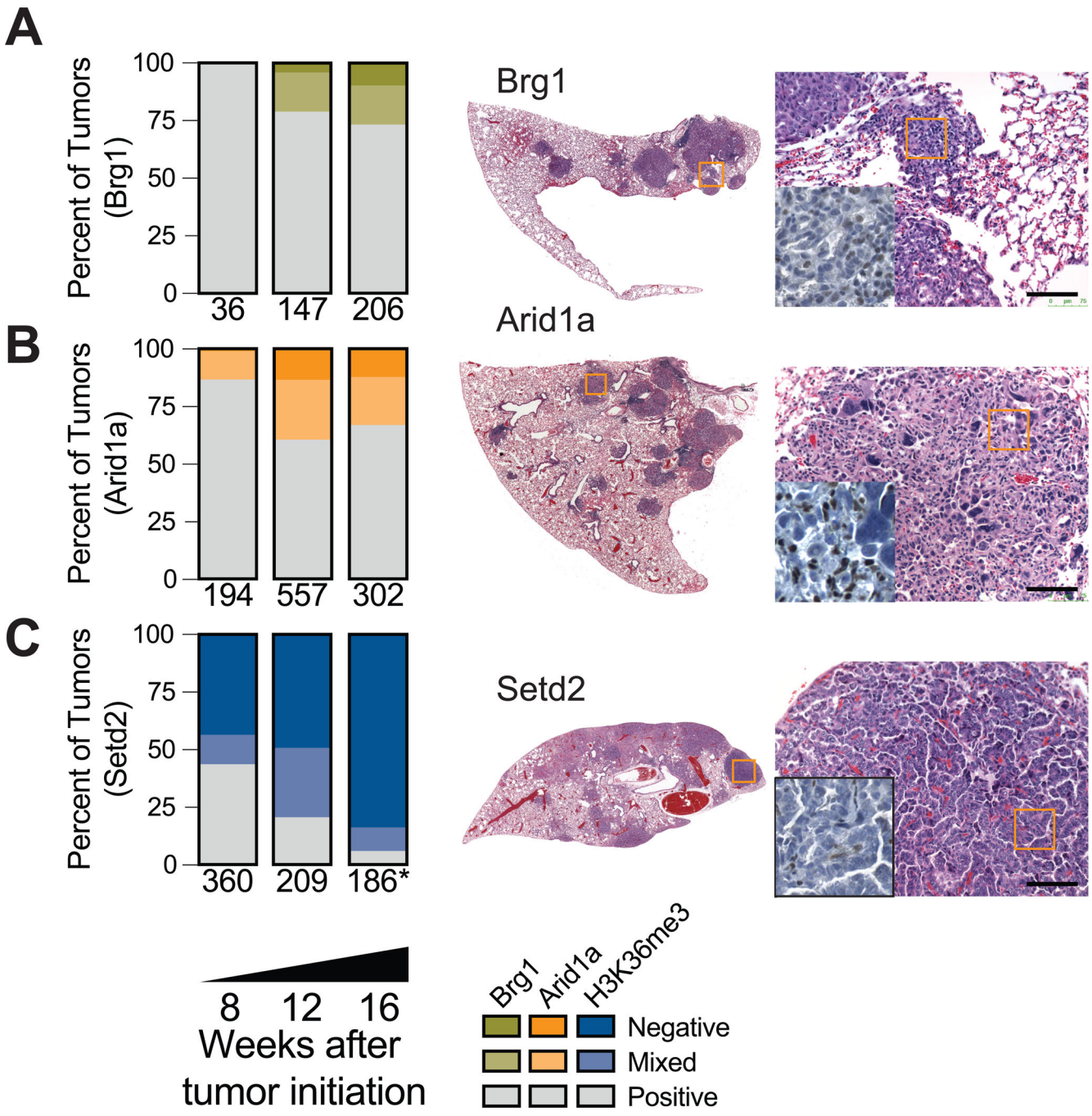

Figure 5.

Loss of Arid1a and Setd2 provide a selective advantage to tumor progression. Left panels: Percent of tumors that are positive, mixed or negative for a) Brg1, b) Arid1a, or c) H3K36me3 expression as determined by IHC in $Kras^{LSL\text{-}G12D/+};p53^{flox/flox}$ mice at 8, 12, and 16 weeks following tumor initiation. * Animals that succumbed to excessive tumor burden prior to the 16 week time point were included in this analysis. Middle panels: Low magnification H&E image of lobe of lung 16 weeks following tumor initiation in $Kras^{LSL\text{-}G12D/+};p53^{flox/flox}$ mice. Right panels: high magnification H&E image of indicated

tumor, inset: IHC for chromatin regulator or histone mark of indicated region of the tumor. Scale bars= 100 μm.

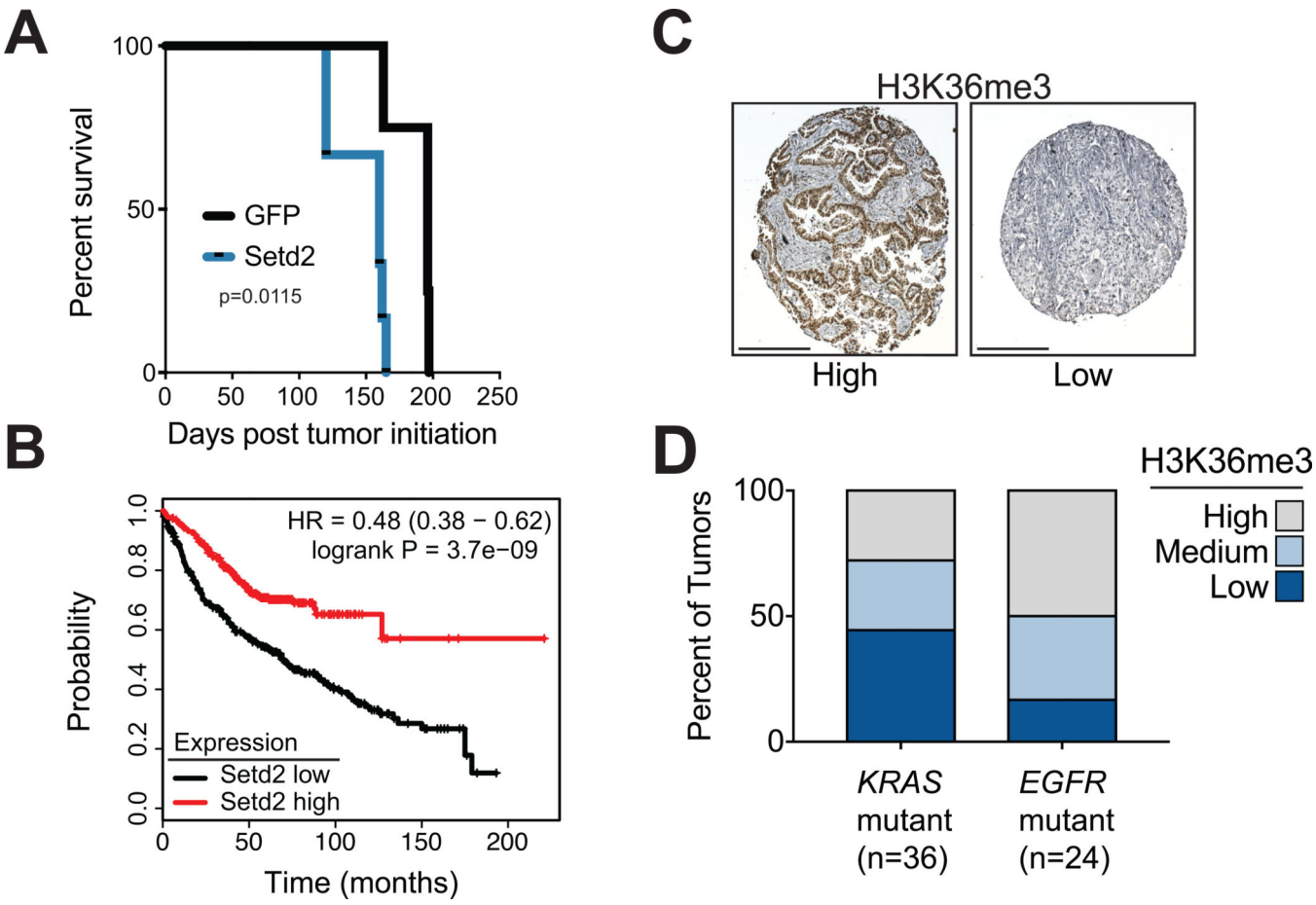

Figure 6.

Loss of Setd2 expression correlates with poor survival in mice and humans and is common in *KRAS* mutant human lung adenocarcinomas. a) Kaplan-Meier survival curves for $Kras^{LSL\text{-}G12D/+};p53^{flox/flox}$ mice given 1.2×10^4 pfu LentiCRISPRv2Cre targeting GFP (n=4) or *Setd2* (n=6). b) Kaplan-Meier survival curves for lung adenocarcinoma patients with Setd2 low (n=360) or Setd2 high (n=360) -expressing tumors [39]. c) Human lung adenocarcinoma tissue microarray stained for H3K36me3. Left panel: H3K36me3-high tumor core, right panel: H3K36me3-low tumor core. Scale bars= 250 μm. d) Percentage of *KRAS* (n=36) or *EGFR* (n=24) mutant human lung adenocarcinomas with high, medium or low H3K36me3 staining. Contingency of H3K36me3 High/Low vs. *KRAS*/*EGFR* mutant tumors, χ^2 5.3, df=1.